GA–A28164

TURBULENT PARTICLE TRANSPORT AS A FUNCTION OF TOROIDAL ROTATION IN DIII-D H-MODE PLASMAS

By

X. Wang[1], S. Mordijck[1], L. Zeng[2], L. Schmitz[2], T.L. Rhodes[2], E.J. Doyle[2], R.J. Groebner[3], O. Meneghini[3], G.M. Staebler[3], and S.P. Smith[3]

This is a preprint of a paper to be submitted for publication in *Plasma Physics and Controlled Fusion*.

[1]College of William & Mary.
[2]University of California.
[3]General Atomics.

Work supported in part by the U.S. Department of Energy under DE-SC0007880[1], DE-FG02-08ER54984[2], and DE-FC02-04ER54698[3]. DIII-D data shown in this paper can be obtained in digital format by following the links at https://fusion.gat.com/global/D3D_DMP.

GENERAL ATOMICS PROJECT 30200

August 2015

GENERAL ATOMICS

Turbulent Particle Transport as a function of toroidal rotation in DIII-D H-mode plasmas

X. Wang

Dept. of Physics, College of William & Mary, Williamsburg, VA, US

E-mail: xwang09@email.wm.edu

S. Mordijck

Dept. of Computer Science, College of William & Mary, Williamsburg, VA, US

L. Zeng, L. Schmitz, T. L. Rhodes, E.J. Doyle

Dept. of Physics and Astronomy, Univ of California, Los Angeles, Los Angeles, CA, US

R. Groebner, O. Meneghini, G.M. Staebler, and S.P. Smith

General Atomics, PO BOX 85608, San Diego, CA, US

Abstract. In this paper we introduce the study of how controlled changes in toroidal rotation affect particle transport and confinement. The toroidal rotation is altered using the co- and counter Neutral Beam Injection (NBI) in low collisionality H-mode plasmas on DIII-D [1] with dominant Electron Cyclotron Heating (ECH). We find that when the $E \times B$ shear is smaller than the linear gyrokinetic growth rate for small $k_\theta \rho_s$ from $\rho = 0.6 - 0.85$, which is observed in a balanced torque injected discharge, particle confinement is lower than in cases where the linear growth rate is smaller than the $E \times B$ shear. In the co- and counter- injected discharges the $E \times B$ shear is larger or close to the linear growth rate and both configurations result in better particle confinement. We observe that there is no correlation between the toroidal rotation shear and the inverse density gradient. The calculated quasi-linear particle flux using TGLF [2] does not agree with experimental observations. In order to measure particle transport, we use a small periodic perturbative gas puff from which we can extract the perturbed diffusion and inward pinch coefficients.

1. Introduction

In this paper we will study the effects of rotation upon particle transport. Toroidal rotation plays a crucial part in stabilizing MHD instabilities, reducing error field penetration as well as determining global confinement in tokamaks [3–7]. The toroidal rotation through the $E \times B$ shear can suppress turbulent transport and thus affects

confinement. On the other hand, shear can also introduce instabilities. With fusion gain strongly dependent on the plasma density, being able to predict the density profile is important for burning plasma regimes [8].

Often in large tokamaks the toroidal rotation is driven by a strong injected torque from the Neutral Beam Injection(NBI). On the other hand, future burning plasma devices, such as ITER, will not have a large level of external injected torque to control the toroidal rotation. Previous research on AUG has shown that there is a correlation between the rotational shear and local density gradient [9, 10]. The changes in rotation shear and changes in the density gradient are the result of changes in dominant mode characteristics and thus turbulence in these plasmas. On DIII-D, to exclude the effects of a change in the dominant linear mode, we kept the input power and fueling levels the same in a set of dedicated discharges. In these discharges, we only change the injected torque, by using a mix of co- and counter beam injection.

Previous research with regards to particle transport concentrates on investigating the role of turbulence and collisionality [9–15]. In a multi-machine comparison, density peaking increases inversely with collisionality. This trend has been confirmed in a 3-point self-similar scan on JET, where collisionality is varied by a factor 5 and the peaking of the density increases when the collisionality is lowered in H-mode [16]. In DIII-D, where collisionality is only varied by a factor 2, no change in peaking is observed [14]. Gyrokinetic simulations of these dimensionless collisionality scaling experiments in DIII-D agree that no increase in particle transport should be observed. To test the role of turbulence upon particle transport, experiments on AUG and DIII-D increase the Te/Ti ratio in order to increase the electron temperature gradient [10, 12, 17, 18]. This results in a local change in turbulence close to mid-radius, where the frequency of the dominant mode is altered. The dominant turbulence mode without Electron Cyclotron Heating (ECH) is originally at mid-radius in the Ion Temperature Gradient (ITG) regime. By adding ECH, which predominantly heats the electrons at low collisionality, the electron temperature gradient increases. This reduces the mode frequency and increases the density gradient until the frequency switches sign and the dominant mode changes to the Trapped Electron Mode (TEM), at which point the density gradient decreases strongly [10]. Simultaneously, AUG also observes changes in the local rotation gradient. A correlation between the toroidal rotational shear, $u' \equiv \frac{R\partial v_{tor}}{v_{i,th}\partial R}$, where R is the major radius, v_{tor} is the toroidal rotation and $v_{i,th}$ is the thermal ion velocity and the inverse density gradient $R/L_n = -\frac{R}{n}\frac{\partial n}{\partial R}$ is observed on AUG [10]. In a set of discharges on DIII-D where the Te/Ti ratio is varied by exchanging NBI heating for ECH, we observe a very weak correlation between R/L_n and u', see figure 1. This motivates us to investigate in more detail how toroidal rotation and rotational shear affect particle transport.

In this paper we keep the power input and mix the same while changing the injected torque using a combination of co-injected and counter-injected beams in predominantly ECH heated plasmas. This allows us to study the effect of rotation, rotational shear, and $E \times B$ shear upon particle transport and confinement. We find that R/L_n at mid-radius does not correlate with u'. While particle confinement is not just determined by

the local gradients at mid-radius, we observe that the discharge with balanced injected torque has the lowest confinement as well as a the smallest R/L_n. A comparison of the calculated quasi-linear particle flux using TGLF with the experimental particle flux shows agreement on a qualitative (not quantitative) level with the co-injected discharges. However, for the balanced and the counter injected discharges, there is not even a qualitative agreement. This indicates that more research needs to be done to modify the transport models in conditions without strong co-torque injection.

First we will discuss the experimental setup of these experiments in section 2 along with the linear stability calculations. In section 3 we will compare the experimental particle flux with quasi-linear TGLF calculations along with the experimentally measured perturbed transport coefficients. Next, in section 4 we will discuss the changes in turbulence characteristics with a focus on the changes in $E \times B$ shear along with the changes in growth rates and density fluctuations. We will conclude with a discussion and short summary.

2. Experiment setup

These experiments were executed in the DIII-D tokamak with major radius, $R \sim 1.67\ m$ and minor radius, $a \sim 0.67\ m$. The heating power is $\sim 5\ MW$ in these H-mode plasmas, with a line averaged density of $3 - 4 \times 10^{19} m^{-3}$, see figure 2. The toroidal magnetic field is $B_T = 1.9\ T$, the plasma current is $I_p = 1.1\ MA$, which results in a $q_{95} \sim 4.2$ and the normalized plasma pressure, $\beta_N = 1 - 1.5$, which allows us to avoid the locked mode limit while operating at low rotation and low density in DIII-D. In Figure 2, at 2000 ms, the initial 3.5 MW NBI power is reduced to 2 MW and 3 MW of ECH power is added. This is also when the torque is altered from purely co-injected to have a quick L to H-mode transition early in the discharge. The torque is varied from 1.1 Nm in one discharge to 0 Nm in the second discharge and $-1.6\ Nm$ in the third. The only fueling comes from the NBI and the plasma-wall interactions, there is no gas puff during the H-mode phase of these discharges.

The change in momentum input results in a change in the core carbon rotation as measured by the Charge Exchange Recombination (CER) system [19]. By changing the torque injection we are able to modify the toroidal rotation profiles. Both the co-injected and the balanced injected discharge rotate in the co-current direction, while the counter injected discharge is close to zero rotation outside $\rho \sim 0.3$ and slightly counter deeper inside, see figure 3. The electron density is measured with the reflectometer system [20]. Electron temperature profiles data come from both the electron cyclotron emission (ECE) [21] and Thomson Scattering system [22]. The changes in rotation affect particle confinement as well the inverse density scale-length. The co- and counter-injected discharge have a similar R/L_n, whereas the balanced torque injected discharge has a much lower inverse density scale length as well as an overall lower electron density. Comparing R/L_n with u' in figure 3 shows that there is no direct correlation between the local changes in u' and the local changes in R/L_n. This lack of correlation for these

3 discharges is emphasized in figure 1, where they represented with a star symbol. The electron temperature profiles are well matched and marginally affected by the changes in toroidal rotation, while the ion temperature profile is slightly higher for the co-injected torque discharge. Especially from $\rho \sim 0.3$ and inward the ion temperature in co-injected discharge is more peaked.

To verify that the small changes in profiles and gradients do not affect the dominant unstable mode, we use TGLF [2] to calculate the linear growth rates and frequencies of the unstables modes. TGLF is a quasi-linear code which has been benchmarked against GYRO [23]. It uses much less computational resources and agrees well with GYRO results for the small wavenumber region where $k_\theta \rho_s < 2$, here k_θ is the poloidal wavenumber, ρ_s is the ion sound radius. The instabilities at small wavenumbers dominate the changes in transport, although non-linear coupling can have a substantial effect on the heat flux [24]. The experimental profiles from figure 3 are used as input to TGLF to calculate the frequency of the most unstable mode (i.e. the mode with the largest growth rate) for $0 < k_\theta \rho_s < 1$, see figure 4. From $\rho = 0.4 - 0.7$ the frequency of the most unstable mode is positive, which means in the electron diamagnetic direction. As a result we can identify it as a Trapped Electron Mode (TEM), which is usually driven by the electron density gradient as well as the electron temperature gradient. Inside $\rho = 0.4$, the counter torque injected discharge remains in the TEM regime, whereas for the two other discharges the frequency becomes negative and in the ion-direction. As a result, the dominant mode is now an Ion Temperature Gradient (ITG) mode. While having the dominant mode in the ITG or TEM regime at certain radial locations does not mean that other modes are unimportant or not present, previous work has shown that there is a correlation between the frequency of the most unstable mode and the local density gradient [10]. In figure 4, we can observe that not only is the frequency of the most unstable mode in the same direction (for $\rho > 0.4$), the magnitude of the frequency is also similar. This allows us to focus on the role of the toroidal rotation in determining particle transport.

3. Particle transport

Using the particle balance equation $\frac{\partial n}{\partial t} = -\nabla\Gamma + S$, where n is the electron density, Γ is the particle flux and S is the fueling source, we can determine the particle flux. Figure 5(a) shows the total particle flux, where a proxy related to the particle confinement time is used to determine the particle source at the plasma edge as a result of plasma-wall interactions. Considering that the core fueling source (NBI fueling is directly proportional to the injected power) for all three discharges is similar, the total particle flux is also similar. Figure 5(b) shows how steady-state transport varies for the three discharges, as represented by an effective diffusion coefficient, $D_{eff} = -\Gamma/(\partial n/\partial r)$. While the particle flux is similar for all three discharges, there are changes in local density gradients (see figure 3), which result in the balanced injected discharge having a much larger effective outward transport than the co and counter-torque injected discharges.

In figure 5 (a) we also calculate the quasi-linear particle flux with TGLF in order to compare it to the experimental results. TGLF calculates the turbulent particle flux at each $k_\theta \rho_s$. By integrating over $k_\theta \rho_s = 0 - 1$ we can extract the quasi-linear particle flux at different radial locations. We find that the calculated quasi-linear flux does not match the experimentally measured flux. In the co-torque injected discharge, the quasi-linear flux is a factor 3 too small, but follows the same trends as the experimental flux. The counter-torque injected discharge has a negative quasi-linear flux between $\rho = 0.5$ and $\rho = 0.6$ and at larger radii the flux increase above experimental values. The quasi-linear particle flux calculations for the balanced-torque injected discharge also exceed the experimental observations outside $\rho = 0.6$. TGLF does not know anything about the fueling sources. Whereas, the calculation of the experimental flux is based on the radial integral of the source, the TGLF calculations are based upon local gradients.

As shown in figure 5, while the particle flux can be similar, particle transport can be very different. While we represented the changes in transport as an effective diffusion coefficient in figure 5, in reality particle transport consists of a pinch, v, as well as diffusion component, D: $\Gamma = -D\frac{\partial n}{\partial r} + vn$. While in a source-less plasma $1/L_n = v/D$, this still does not allow us to extract the separate contributions of D and v. In order to measure the pinch and diffusion contributions, separately we have to rely on the use of a perturbative technique. Since the 1980s and again in more recent years (due to improved temporal and spatial diagnostic capabilities), a modulated gas puff technique has been employed to measure the perturbed pinch, v_p and the perturbed diffusion coefficient, D_p [14, 25–30]. Adding a periodic small gas puff modulates the density profile with a fixed periodicity. We can extract both the amplitude and the phase of this modulation using Fourier analysis. Using the perturbed continuity equation as shown by Takenaga et al. [31], the perturbed D_p and v_p can then be expressed in terms of the measured phase and amplitude. We refer the reader to previous work by Doyle et al. [14] and Mordijck et al. [25,26] with more details on this technique for DIII-D plasmas. Figure 6 shows the measured D_p and v_p of the three discharges. While the co-torque discharge and balanced torque discharge have similar transport coefficients, the counter-torque discharge has a stronger convective inward pinch. This matches well with the observation in Figure 3(c) that the counter-torque discharge has the highest electron density profile.

4. Turbulence and $E \times B$ shear

Earlier we showed the there is no correlation between u' and R/L_n in a database of DIII-D plasmas (see figure 1), nor is there a correlation between u' and R/L_n in the set of three dedicated experiments in which the torque injection was varied (to vary the toroidal rotation), while keeping other parameters that affect turbulence the same. While u' acts as an off-diagnonal term in determining particle transport, its influence is small for main ions and electrons. However, toroidal rotation can also indirectly affect particle transport, through its contribution to the radial electric field E_r and thus the $E \times B$ shearing rate [4]:

$$qE_r = q(Z_i e n_i)^{-1}\nabla P_i - qv_{\theta_i}B_\phi + qv_{\phi i}B_\theta \quad (1)$$

$$\omega_{E\times B} = \frac{(RB_\theta)^2}{B}(\frac{\partial}{\partial\Psi})\frac{E_r}{RB_\theta} \quad (2)$$

Here, Z_i is the net particle charge of species i, P_i is plasma pressure, v_i is the plasma velocity and θ and ϕ denote poloidal and toroidal direction respectively, B is the magnetic field and Ψ is the poloidal flux. Figure 7 shows for the same database as figure 1 using the same profiles that there is a very weak correlation for $\rho = 0.5 - 0.7$ between the local $E \times B$ shearing rate and the local peaking of the density. While the density gradient is also input to $\omega_{E\times B}$, there were large variations in the electron and ion temperature gradients as well as rotation to eliminate any trends. In the next section we will study the role of the $E \times B$ shearing rate in more detail for the discharges in which we varied the torque injection.

4.1. Growth rate versus ExB shearing rate

Gradients drive micro-instabilities in tokamak plasmas, which result in the creation of eddies that drive turbulent transport. These eddies can be torn apart or suppressed by a sheared flow [4,5,32–34]. Sheared flow, such as the $E\times B$ shear, affects turbulence in two ways [4]; through nonlinear decorrelation, which includes the reduction in the turbulence radial correlation length, phase, and fluctuation size; or through linear stabilization, which enhances the damping of turbulence by coupling the unstable modes to nearby, stable modes, thus improving the overall stability of the system. The $E \times B$ shear flow has a strong poloidal component (see equation 2), which can suppress turbulent transport. Whereas in the pedestal region, the radial electric field (and thus the $\omega_{E\times B}$ rate) is dominated by the pressure gradient, deeper inside the core, the toroidal rotation plays an important role [35]. In our set of three discharges, due to the changes in input torque, we change the toroidal rotation and the $E \times B$ shear, see figure 8. From $\rho = 0.6 - 0.8$ we can observe the effect of the difference in toroidal rotation, outside $\rho = 0.8$ the changes in the pressure gradient dominate and inside $\rho = 0.6$ the shearing rate is small and the local difference between the discharges are related to fitting choices. The discharge with balanced torque injection has the lowest $\omega_{E\times B}$, while the co- and counter torque injected discharges have a higher shearing rate from $\rho = 0.6 - 0.8$.

The shearing rate by itself can be an indication of whether turbulent transport will be suppressed, but a better indication is to compare the linear growth rate of the instabilities with the $E \times B$ shearing rate. In a simplified picture, without including non-linear effects, the rule of thumb is that if the linear growth rate is smaller than the shearing rate, the mode will be suppressed, whereas if the linear growth rate is larger than the shearing rate, the mode will not be suppressed by the shearing rate. Figure 9 shows the maximum linear growth rates for $k_\theta\rho_s = 0.1 - 0.5$ along with $\omega_{E\times B}$. For the co- (figure 9(a)) and the counter-torque injected cases (figure 9(b)) $\omega_{E\times B}$ is larger than or of similar magnitude as the maximum linear growth rate. Whereas for the balanced

torque injected discharge, the average linear growth rate is significantly larger than the $E \times B$ shearing rate from $\rho = 0.6 - 0.85$. This suggests that the balanced injected discharge will not be able to suppress turbulent transport outside the mid-radius up to the top of the pedestal as well as the co- and counter torque injected discharges.

4.2. Density fluctuations

To investigate the changes in turbulence we compare the density fluctuations measured by the Doppler BackScattering [36], see figure 10. The DBS measures density fluctuations at the intermediate scale, in this case the range in $k_\theta \rho_s = 1.6 - 2.8$. This intermediate scale is typically associated with the TEM unstable regime. We observe in figure 10 (a) that density fluctuations for the balanced and co-torque injected discharges have similar values for $\tilde{n}/n$, whereas the counter-torque injected discharge has higher $\tilde{n}/n$ from $\rho = 0.7 - 0.9$. This is also the radial location where a strong increase in the perturbed particle pinch measurement is observed for the counter-torque injected discharge, see figure 6.

Figure 10 (b) shows the average linear growth rate for the same $k_\theta \rho_s$ scale. In a simplified linear picture, the growth rates should be equivalent to the actual density fluctuations at the same scale. Accounting for the fact that there is no data for the co and balanced injected discharge, it is impossible to compare the trends between $\rho = 0.7 - 0.9$. Outside this area, the linear growth rates seem to be in agreement qualitatively with the observed density fluctuations. The values for the balanced torque injected discharge show no indication to increase between $\rho = 0.7 - 0.9$ as shown in the simulations, but neither an increase nor decrease in the density fluctuation amplitude can be confirmed.

5. Discussion

In this paper we seek to study the effects of rotation upon particle transport. On AUG, when the frequency of the dominant unstable mode is varied by changing the Te/Ti ratio, a correlation between R/L_n and u' is observed [10]. In this paper, we do not observe such a correlation in plasmas in which the ratio of Te/Ti was varied. In a dedicated study to investigate the role of the toroidal rotation upon particle transport, we find that if the frequency of the dominant unstable mode remains similar and only the input torque is varied, there is no correlation between u' and R/L_n.

The changes in toroidal rotation however feed into the $E \times B$ shearing rate and by varying the injected torque we were able to vary the $E \times B$ shear substantially from $\rho = 0.6 - 0.8$. The ability of the $E \times B$ shear from mid-radius to the top of the pedestal to regulate particle confinement was also found previous in QH-mode [37] and during the application of Resonant Magnetic Perturbations (RMPs) [25]. In both previous results, when the linear growth rate for small $k_\theta \rho_s$ from mid-radius to the top of the pedestal is larger than the $E \times B$ shear, a reduction in particle confinement is observed. While

in the QH-mode and the RMP H-mode experiments on DIII-D, the underlying linear stability is altered (due to changes in temperature gradients), in this dedicated set of three discharges the gradients are similar and, as a result, the frequency of the most unstable mode is similar for all three discharges in which the torque was varied.

However as shown in this paper, the linear and quasi-linear gyrokinetic simulations show some disagreement with experimental observations on microscopic (no correlation between linear growth rates and experimental density fluctuations) as well as macroscopic scales (experimental and quasi-linear particle flux do not match). One explanation could be that non-linear effects play an important role and that full non-linear gyrokinetic simulations would result in better agreement. For example, non-linear multi-scale gyrokinetic simulations have already shown to increase the heat flux by 30% in comparison with ITG-only non-linear gyrokinetic simulations [38]. As of yet, it is unclear whether fully non-linear multi-scale gyrokinetic simulations would result in an increase of the particle flux by a factor 3 or result in a reversal in the particle flux from inward to outward or a decrease in particle flux at other radii. Future work will include full non-linear gyrokinetic simulations to assess how much they diverge from the quasi-linear simulations with respect to particle transport.

The perturbed transport coefficients indicate that the changes in transport are not just the result of changes in outward diffusion, but also inward convection. However, these are perturbed transport coefficients and it is unclear whether they accurately reflect the steady-state transport coefficients. Although the perturbations to the density are small, this can still affect the local gradients. One interesting observation is that we measure in the counter-torque plasma a strong inward particle pinch, which occurs at the same radii as the strong increase in intermediate scale density fluctuations. A similar correlation between a strong increase in perturbed inward particle pinch and an increase in intermediate scale density flctuations is also observed in plasmas in which the Te/Ti is varied [26]. Although perturbed techniques to measure particle transport coefficients have been around since the 80s, more work needs to be done to connect them to steady-state transport coefficients.

6. Summary

In this paper we presented the first dedicated study as to how particle transport and confinement change when the toroidal rotation is altered. We varied the toroidal rotation by changing the injected torque and we find that there is a correlation between R/L_n and the $E \times B$ shear. When the $E \times B$ shear is lower than the linear growth rate at small $k_\theta \rho_s$ outside mid-radius, this results in a decrease in particle confinement. As a result, the discharge without external net torque resulted in the lowest particle confinement of the three discharges. Perturbed transport coefficients indicate that changes in transport are not just related to an increase in outward diffusion. In the counter-torque injected discharge, which has the best particle confinement a strong increase in the perturbed inward pinch is observed at the plasma edge and intermediate scale density fluctuation

at the same radius. Finally, we observe that quasi-linear gyrokinetic simulations of the particle flux using TGLF do not match experimental observations.

Acknowledgment

This material is based upon work supported by the U.S. Department of Energy, Office of Science, Office of Fusion Energy Sciences, using the DIII-D National Fusion Facility, a DOE Office of Science user facility, under Awards DE-SC0007880, DE-FC02-04ER54698, and DE-FG02-08ER54984. DIII-D data shown in this paper can be obtained in digital format by following the links at https://fusion.gat.com/global/D3D_DMP.

[1] J. L. Luxon. A design retrospective of the DIII-D tokamak. *Nuclear Fusion*, 42(5):614, 2002.

[2] G. M. Staebler, J. E. Kinsey, and R. E. Waltz. Gyro-Landau fluid equations for trapped and passing particles. *Physics of Plasmas*, 12:102508, 2005.

[3] R. Fitzpatrick and T. C. Hender. The interaction of resonant magnetic perturbations with rotating plasmas. *Physics of Fluids B: Plasma Physics (1989-1993)*, 3(3):644–673, 1991.

[4] K. H. Burrell. Effects of ExB velocity shear and magnetic shear on turbulence and transport in magnetic confinement devices. *Physics of Plasmas*, 4:1499, 1997.

[5] H. Biglari, P. H. Diamond, and P. W. Terry. Influence of sheard poloidal rotation on edge turbulence. *Physics of Fluids B*, 2(1):1–4, 1990.

[6] N Aiba, J Shiraishi, and M Hirota. Impact of plasma rotation on the linear physics of resistive wall modes in tokamaks. *Plasma Physics and Controlled Fusion*, 55(7):074002, 2013.

[7] I T Chapman, S D Pinches, J P Graves, R J Akers, L C Appel, R V Budny, S Coda, N J Conway, M de Bock, L-G Eriksson, R J Hastie, T C Hender, G T A Huysmans, T Johnson, H R Koslowski, A Krmer-Flecken, M Lennholm, Y Liang, S Saarelma, S E Sharapov, I Voitsekhovitch, the MAST, TEXTOR Teams, and JET EFDA Contributors. The physics of sawtooth stabilization. *Plasma Physics and Controlled Fusion*, 49(12B):B385, 2007.

[8] J. Lawson. Some criteria for a power producing thermonuclear reactor. *Proceedings of the Physical Society. Section B*, 70(1):6–10, 1957.

[9] C. Angioni, R. M. McDermott, F. J. Casson, E. Fable, A. Bortolon, R. Dux, R. Fischer, Y. Podoba, T. Putterich, F. Ryter, E. Viezzer, and ASDEX Upgrade Team. Intrinsic toroidal rotation, density peaking, and turbulence regimes in the core of tokamak plasmas. *Physics Review Letters*, 107:215003, 2011.

[10] C. Angioni, Y. Camenen, F. J. Casson, E. Fable, R. M. McDermott, A. G. Peeters, and J. E. Rice. Off-diagonal particle and toroidal momentum transport: a survey of experimental, theoretical and modelling aspects. *Nuclear Fusion*, 52:114003, 2012.

[11] C. Angioni, H. Weisen, O.J.W.F. Kardaun, M. Maslov, A. Zabolotsky, C. Fuchs, L. Garzotti, C. Giroud, B. Kurzan, P. Mantica, A.G. Peeters, J. Stober, the ASDEX Upgrade Team, and contributors to the EFDA-JET Workprogramme. Scaling of density peaking in H-mode plasmas based on a combined database of AUG and JET observations. *Nuclear Fusion*, 47(9):1326, 2007.

[12] C. Angioni, J. Candy, E. Fable, M. Maslov, A. G. Peeters, R. E. Waltz, and H. Weisen. Particle pinch and collisionality in gyrokinetic simulations of tokamak plasma turbulence. *Physics of Plasmas*, 16(6):060702, 2009.

[13] M. Greenwald, C. Angioni, J.W. Hughes, J. Terry, and H. Weisen. Density profile peaking in low collisionality H-modes: comparison of Alcator C-Mod data to ASDEX Upgrade/JET scalings. *Nuclear Fusion*, 47(9):L26, 2007.

[14] E. J. Doyle, L. Zeng, G. M. Staebler, T. E. Evans, T. C. Luce, G. R. McKee, S. Mordijck, R. A. Moyer, W. A. Peebles, C. C. Petty, and T. L. Rhodes. Particle transport results from collisionality scans and perturbative experiments on DIII-D. In *Conference proceeding of 24th IAEA Fusion Energy Conference San Diego, USA*, 2012.

[15] H Weisen, A Zabolotsky, M Maslov, M Beurskens, C Giroud, D Mazon, and JET-EFDA contributors. Scaling of density peaking in JET H-modes and implications for ITER. *Plasma Physics and Controlled Fusion*, 48(5A):A457, 2006.

[16] T. Tala, P. Mantica, A. Salmi, C. Bourdelle, C. Giroud, J. Hillesheim, C. Maggi, L. Meneses, M. Maslov, S. Menmuir, S. Moradi, S. Mordijck, V. Naulin, H. Nordman, J. Juul Rasmussen, G. Sips, A. Sirinelli, M. Tsalas, H. Weisen, and JET contributors. Dimensionless collisionality scans for core particle transport in JET. In *42nd EPS Conference on Plasma Physics*, 2015.

[17] C. Angioni, A.G. Peeters, X. Garbet, A. Manini, F. Ryter, and ASDEX Upgrade Team. Density response to central electron heating: theoretical investigations and experimental observations in ASDEX Upgrade. *Nuclear Fusion*, 44(8):827, 2004.

[18] C. Angioni, R.M. McDermott, E. Fable, R. Fischer, T. Ptterich, F. Ryter, G. Tardini, and the ASDEX Upgrade Team. Gyrokinetic modelling of electron and boron density profiles of H-mode

plasmas in ASDEX upgrade. *Nuclear Fusion*, 51(2):023006, 2011.

[19] B. A. Grierson, K. H. Burrell, W. M. Solomon, and N. A. Pablant. Deuterium velocity and temperature measurement on the DIII-D tokamak. *Review of Scientific Instruments*, 81:10D735, 2010.

[20] L. Zeng, G. Wang, E. J. Doyle, T. L. Rhodes, W. A. Peebles, and Q. Peng. Fast automated analysis of high-resolution reflectometer density profiles on DIII-D. *Nuclear Fusion*, 46:S677, 2006.

[21] D. D. Truong and M. E. Austin. High spatial resolution upgrade of the electron cyclotron emission radiometer for DIII-D tokamak. *Review of Scientific Instruments*, 85:11D814, 2014.

[22] D. M. Ponce-Marquez, B. D. Bray, T. M. Deterly, C. Liu, and D. Eldon. Thomson scattering diagnostic upgrade on DIII-D. *Review of Scientific Instruments*, 81:10D525, 2010.

[23] J. Candy and R. E. Waltz. An Eulerian gyrokinetic-Maxwell solver. *Journal of Computational Physics*, 186:545–581, 2003.

[24] N. T. Howard, A. E. White, M. Greenwald, C. Holland, and J. Candy. Multi-scale gyrokinetic simulation of Alcator C-Mod tokamak discharges. *Physics of Plasmas*, 21:032308, 2014.

[25] S. Mordijck, E. J. Doyle, G. R. McKee, R. A. Moyer, T. L. Rhodes, L. Zeng, N. Commaux, M. E. Fenstermacher, K. W. Gentle, H. Reimerdes, O. Schmitz, W. M. Solomon, G. M. Staebler, and G. Wang. Changes in particle transport as a result of resonant magnetic perturbations in DIII-D. *Physics of Plasmas*, 19:5, 2012.

[26] S. Mordijck, X. Wang, E. J. Doyle, T. L. Rhodes, L. Schmitz, L. Zeng, G. Staebler, C. C. Petty, W-H. Ko, B. Grierson, W. Solomon, T. Tala, A. Salmi, P. H. Diamond, and G. R. McKee. Particle transport in low-collisionality H-mode plasma on DIII-D. *Submitted*, 2014.

[27] J. O'Rourke, F.G. Rimini, and D.F.H. Start. Perturbative measurements of the electron transport matrix using ICRF power modulation. *Nuclear Fusion*, 32(10):1861, 1992.

[28] K W Gentle, G Cima, H Gasquet, G A Hallock, P E Phillips, W L Rowan, C Watts, O Gehre, and the ASDEX-U Team. Characteristics of equilibrium and perturbed transport coefficients in tokamaks. *Physica Scripta*, 52(4):411, 1995.

[29] N J Lopes Cardozo. Perturbative transport studies in fusion plasmas. *Plasma Physics and Controlled Fusion*, 37(8):799, 1995.

[30] A. Jacchia, P. Mantica, F. De Luca, and G. Gorini. Determination of diffusive and nondiffusive transport in modulation experiments in plasmas. *Physics of Fluids B*, 3(11):3033–3040, 1991.

[31] H. Takenaga, K. Nagashima, A. Sakasai, T. Oikawa, and T. Fujita. Determine of particle transport coefficients in reversed shear plasma of JT-60U. *Plasma Physics and Controlled Fusion*, 40:183, 1998.

[32] E. J. Doyle, C. L. Rettig, K. H. Burrell, P. Gohil, R. J. Groebner, T. K. Kurki-Suonio, R. J. La Haye, R. A. Moyer, T. H. Osborne, W. A. Peebles, R. Philipona, T. L. Rhodes, T. S. Taylor, and J. G. Watkins. Turbulence and transport reduction mechanisms in the edge and interior of DIII-D H-mode plasmas. *Plasma Physics and Controlled Fusion*, 1:235, 1993.

[33] P. W. Terry. Suppression of turbulence and transport by shear flow. *Reviews of Modern Physics*, 72:109, 2000.

[34] R. E. Waltz, G. D. Kerbel, and J. Milovich. Toroidal gyro-Landau fluid model turbulence simulations in a nonlinear ballooning mode representation with radial modes. *Physics of Plasmas*, 1:2229, 1994.

[35] R. M. McDermott, B. Lipschultz, J. W. Hughes, P. J. Catto, A. E. Hubbard, I. H. Hutchinson, R. S. Granetz, M. Greenwald, B. LaBombard, K. Marr, M. L. Reinke, J. E. Rice, D. Whyte, and Alcator C-Mod Team. Edge radial electric field structure and its connections to H-mode confinement in Alcator C-Mod plasmasa. *Physics of Plasmas*, 16(5):056103, 2009.

[36] J. C. Hillesheim, W. A. Peebles, T. L. Rhodes, L. Schmitz, T. A. Carter, P. A. Gourdain, and G. Wang. A multichannel, frequency-modulated, tunable Doppler backscattering and reflectometry system. *Review of Scientific Instruments*, 80:083507, 2009.

[37] A.M. Garofalo, W.M. Solomon, J.-K. Park, K.H. Burrell, J.C. DeBoo, M.J. Lanctot, G.R. McKee,

H. Reimerdes, L. Schmitz, M.J. Schaffer, and P.B. Snyder. Advances towards QH-mode viability for ELM-stable operation in ITER. *Nuclear Fusion*, 51(8):083018, 2011.

[38] N. T. Howard, A. E. White, M. L. Reinke, M. Greenwald, C. Holland, J. Candy, and J. R. Walk. Validation of the gyrokinetic model in ITG and TEM dominated L-mode plasmas. *Nuclear Fusion*, 53:123011, 2013.

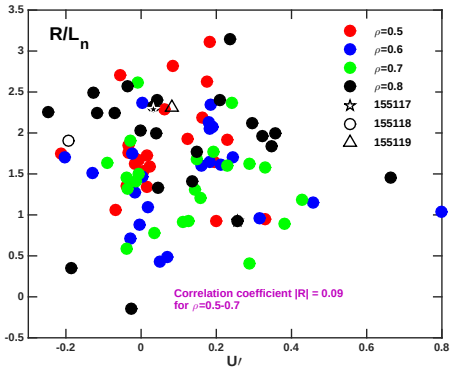

Figure 1. [Color online] Normalized density gradient, R/L_n as a function of toroidal rotation shear $u' = -\frac{R}{v_{i,th}}\frac{\partial v_{tor}}{\partial R}$ for low density H-mode discharges in which the ratio of T_e/T_i was varied. (Data from DIII-D)

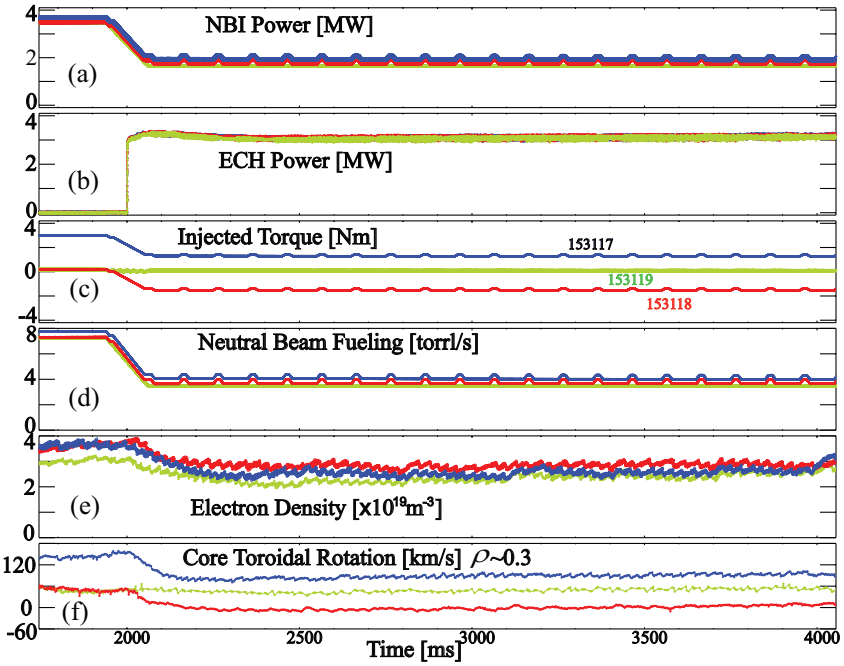

Figure 2. [Color online] Time evolution of three DIII-D H-mode discharges with different torque injection.(a) The NBI heating power for each discharge and the (b) ECH injected power are kept the same. (c) The NBI torque injection is varied from co- to counter-injected. (d) The fueling from the NBI is the same for all three discharges (e) The change in torque injection results in different line averaged electron density. (f) The core carbon rotation close to $\rho = 0.3$ varies from co-rotating to zero rotation.

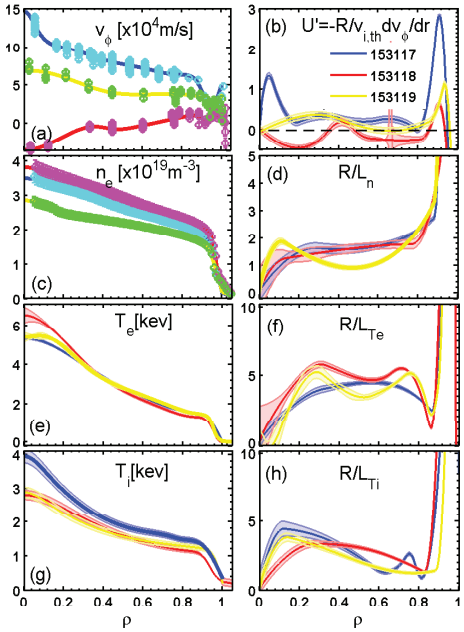

Figure 3. [Color online] Experimental fitted profiles and their normalized gradients for all three discharges (blue = co, yellow = balanced and red = counter injected NBI). (a-b) Due to the different injected torque the toroidal carbon rotation and its normalized gradient, u' are very different for all three discharges. (c-d) The electron density is the highest for the counter injected discharge and the lowest for the balanced injection. R/L_n for the co- and counter injected discharge are fairly similar. (e-f) The electron temperature profile is fairly similar for all three discharges outside $rho \sim 0.2$. (g-h) The ion temperature is slightly higher for the co-injected discharge in comparison with the two other discharges.

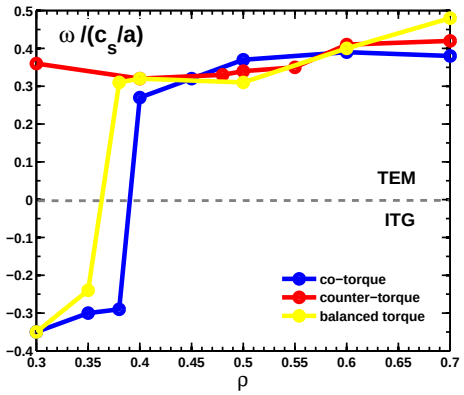

Figure 4. [Color online] Frequency of the most unstable mode for $0 < k_\theta \rho_s < 1$ by TGLF. All three discharge are in TEM regime outside $\rho = 0.4$ ($\omega > 0$). Inside $\rho = 0.4$, the counter torque injected plasma is still in the TEM regime, whereas the other two discharges change to the ITG regime.

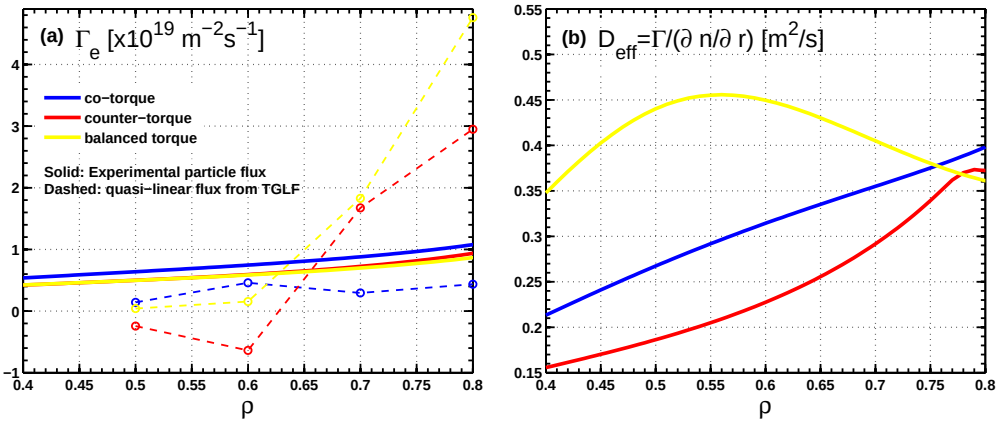

Figure 5. [Color online] (a) Total electron particle flux (solid lines) determined using particle balance; the dashed lines are the calculated quasi-linear calculated electron flux with TGLF. (b) Effective transport as represented by an effective diffusion coefficient, $D_{eff} = \Gamma/(\partial n/\partial r)$ for the 3 discharges.

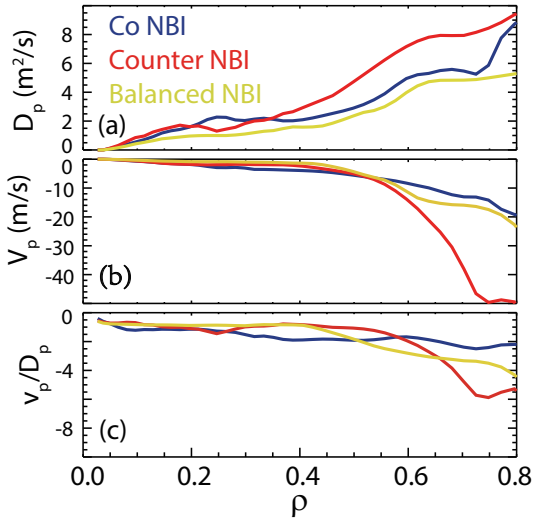

Figure 6. [Color online] Perturbative transport measurement for the three discharges: (a) Diffusive coefficients are similar in magnitude (b) Convective coefficients show that counter-torque discharge has a much larger inward pinch than the other two discharges outside $\rho = 0.6$. (c) The ratio of v_p/D_p.

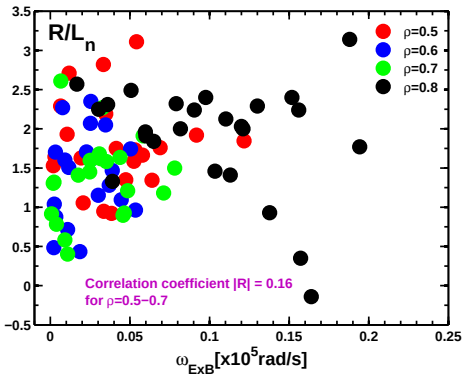

Figure 7. [Color online] Normalized density gradient as a function of $E \times B$ shearing rate for the same database of H-mode discharges as figure 1. The different colors represent different radial locations.

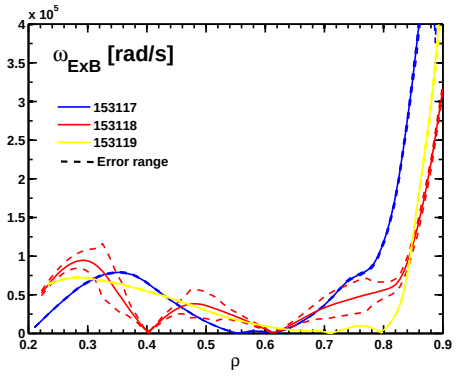

Figure 8. [Color online] $E \times B$ shearing rates (using Hahm-Burrell [4]) for the three discharges with different torque injection.

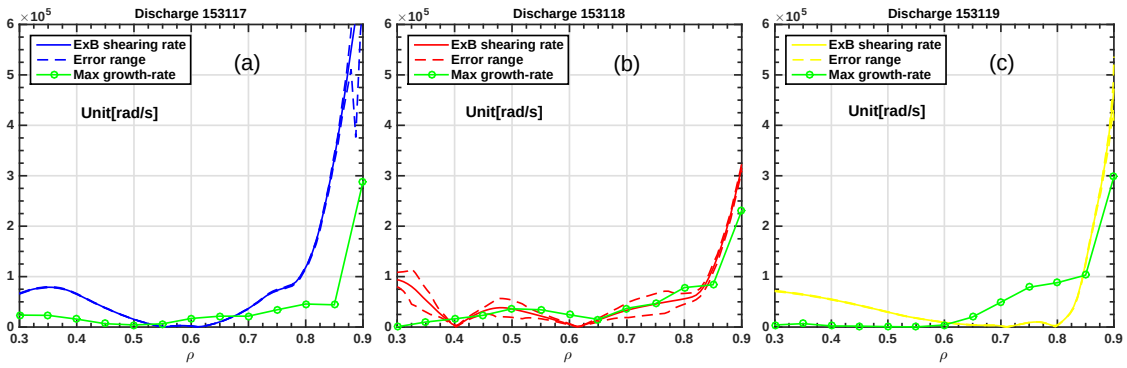

Figure 9. [Color online] $E \times B$ shearing rates versus the maximum growth rates for $k_\theta \rho_s = 0.1 - 0.5$. Three $E \times B$ shearing rates are labeled with different colors: (a) co-torque (Blue), (b) counter-torque (Red), and (c) balanced torque (Yellow). All the growth rates are represented by the green lines.

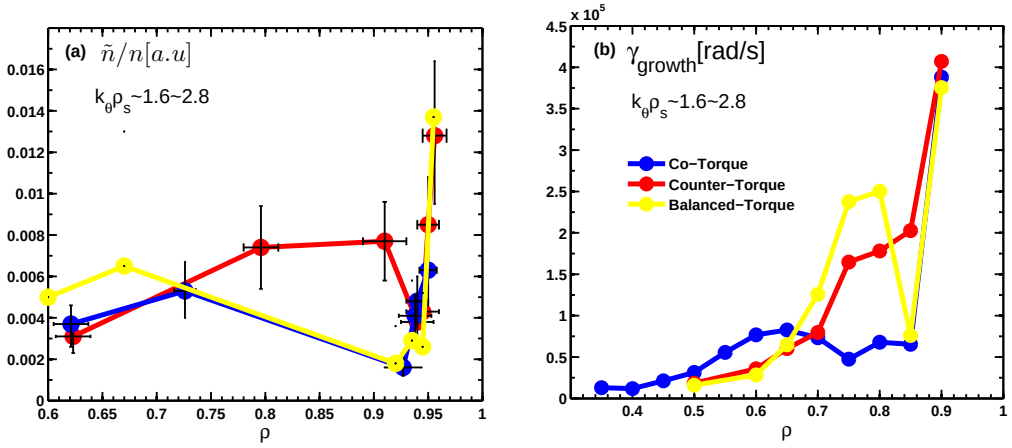

Figure 10. (a) Density fluctuations measured by DBS at intermediate scale ($k_\theta\rho_s = 1.6-2.8$) for all three discharges. (b) The average linear growth rate for $k_\theta\rho_s = 1.6-2.8$.